doi:10.1017/S1431927615013410

The Differential Algebra Based Multiple Level Fast Multipole Algorithm for 3D Space Charge Field Calculation and Photoemission Simulation

He Zhang[1], Jenni Portman[2], Zhensheng Tao[2], Phillip Duxbury[2], Chong-Yu Ruan[2], Kyoko Makino[2] and Martin Berz[2]

[1.] Center for Advanced Studies of Accelerators, Jefferson Lab, Newport News, VA, USA
[2.] Department of Physics and Astronomy, Michigan State University, East Lansing, MI, USA

Coulomb interaction between charged particles inside a bunch is one of the most important collective effects in beam dynamics, becoming even more significant as the energy of the particle beam is lowered to accommodate analytical and low-Z material imaging purposes such as in the time resolved Ultrafast Electron Microscope (UEM) development currently underway at Michigan State University. Space charge effects are the key limiting factor in the development of ultrafast atomic resolution electron imaging and diffraction technologies [1-4] and are also correlated with an irreversible growth in rms beam emittance due to fluctuating components of the nonlinear electron dynamics. In the short pulse regime used in the UEM, space charge effects also lead to virtual cathode (VC) formation in which the negative charge of the electrons emitted at earlier times, combined with the attractive surface field, hinders further emission of particles and causes a degradation of the pulse properties. Space charge and virtual cathode effects and their remediation are core issues for the development of the next generation of high-brightness UEMs [5-9]. Since the analytical models are only applicable for special cases, numerical simulations, in addition to experiments, are usually necessary to accurately understand the space charge effect. In this paper we will introduce a grid-free differential algebra (DA) based multiple level fast multipole algorithm (MLFMA), which calculates the 3D space charge field for n charged particles in arbitrary distribution with an efficiency of $O(n)$ [10], and the implementation of the DA based MLFMA to a simulation code for space charge dominated photoemission process.

The key idea of the Fast Multipole Method (FMM) is to represent the potential of groups of source particles that are far away from the observer in terms of expansions, taking advantage of the fact that the Coulomb potential decreases with the distance. In order to evaluate the electrostatic field due to an arbitrary distribution of charges, we divide the charges into groups and evaluate the interactions between the groups far away by using a multipole expansion, while the interactions between nearby particles are calculated directly using the pairwise formula for the Coulomb potential. The domain containing the charges is divided into boxes of different sizes depending on the charge density so that on average each box includes a similar number of particles, leading to the multiple level version of the FMM [10].

Relations between boxes can be represented as a hierarchical tree, as shown in Figure 1. Small boxes generated by subdividing a large box are called child boxes of the large box, and the large box is called the parent box of the small ones. The boxes that have no child boxes are called childless boxes. If the distance from any observer to a source box is larger than the side length of the source box, the field on the observer can be represented by the multipole expansion located inside the source box. If the distance from any source particle to the observer box is larger than the side length of the observer box, its contribution to the field inside the observer box can be represented as a local expansion inside the observer box. Each box is treated as both a source box and an observer box, thus we will calculate both the multiple expansion and the local expansion for the box. For a childless box the multipole expansion is calculated from the charges inside it, while for a parent box the multipole expansion is calculated from

the multipole expansions of its child boxes. Local expansion of far enough boxes can be either calculated from the charges inside a childless box or from the multipole expansion of a parent box, and child boxes inherit the local expansions from their parent boxes. The general strategy is then to calculate the multipole expansions for all the childless boxes and then transfer it into multipole expansions of the parent boxes, going up the tree. Once this is done, the local expansions for all the boxes can be calculated from the highest level of the tree to the lowest level. The field on each particle in the childless boxes is then given by a sum of two parts: the contribution of the nearby particles is calculated using the pairwise formula for the Coulomb potential, while the field due to the particles far away is calculated from the multipole expansions and/or the local expansions. For more details on the FMM see [10].

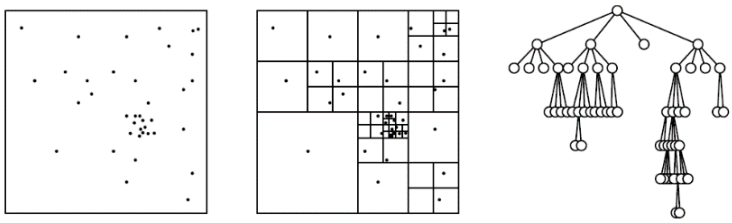

Figure 1. Decomposition of the space using the multiple level algorithm and the corresponding tree structure that represents the hierarchical relationships between boxes.

The key step in the above procedure is the calculation of the multipole and local expansions. Many different approaches have been developed to treat the Coulomb interaction, such as spherical harmonic functions, tensors, etc. [10-13]. In the present work, we use the differential algebra (DA) technique [14] where all the expansions are represented as DA vectors. The code to perform this was developed as a package for COSY INFINITY [15,16], in which DA is supported as an advanced data type to carry out the arithmetic for elementary operations and intrinsic functions of DA vectors, thus the Taylor expansion of any well-defined function can be calculated as a DA vector with properly selected (small) DA variables. Any translation of the expansions (e.g. from child to parent box) simply becomes a composition of the expansions with the map corresponding to the translation, where the composition is also a DA elementary operation in COSY INFINITY.

While a detailed derivation of the DA implementation of the MLFMA is beyond the scope of this paper and can be found in [17,18], we will introduce the key steps necessary for the calculation of the multipole and local expansions using DA. First let us consider a childless box with n particles with charge q_i located at $\mathbf{r}_i(x_i,y_i,z_i)$, then the electrostatic potential at a point $\mathbf{r}(x,y,z)$ outside the box can be expressed as

$$\phi = \sum_{i=1}^{n} \frac{q_i}{|\mathbf{r}_i - \mathbf{r}|} = d \cdot \phi_{\mathrm{M}}$$

with $\phi_{\mathrm{M}} = \sum_{i=1}^{n} \left(q_i / \sqrt{1 + r_i^2 d^2 + 2\mathbf{r}_i \cdot \mathbf{d}} \right)$, $\mathbf{d} = \mathbf{r} / r^2$ and d is the norm of $\mathbf{d}$. Choosing d_x, d_y, and d_z, the components of $\mathbf{d}$, as DA variables, ϕ_M can be expressed as a DA vector. This formula can be used to calculate the multipole expansions of all the childless boxes.

Next, to calculate the multipole expansion of a parent box, we simply translate the multipole expansions of its child boxes to the center of the parent box and sum over them. Without losing generality, let us assume that the center of the child box is at $\mathbf{O}(0,0,0)$ and the center of the parent box is located at

$\mathbf{r}_{\mathrm{o}}'(x_{\mathrm{o}}', y_{\mathrm{o}}', z_{\mathrm{o}}')$. In the parent box frame, new DA variables can be chosen as $\mathbf{d}' = (\mathbf{r} - \mathbf{r}_{\mathrm{o}}')/r'^2 = \mathbf{r}'/r'^2$, where $\mathbf{r}(x, y, z)$ is the position of an arbitrary observer far away and $\mathbf{r}' = \mathbf{r} - \mathbf{r}_{\mathrm{o}}'$. The transfer map between the new DA variables and the old DA variables, which we refer to as M_1, is then given by $\mathbf{d} = (\mathbf{d}' + d'^2\mathbf{r}_{\mathrm{o}}') \cdot R$, with $R = 1/(1 + r_{\mathrm{o}}'^2 d'^2 + 2\mathbf{r}_{\mathrm{o}}' \cdot \mathbf{d}')$. The potential in the new frame has the same format as in the old frame and, using $\phi_{\mathrm{M}}' = \sqrt{R} \cdot (\phi_M \circ M_1)$, can be written as

$$\phi' = \phi \circ M_1 = d' \cdot \phi_M',$$

where "$\circ$" denotes the composition of two maps. This formula can be used to calculate the multipole expansions of all the parent boxes.

Having calculated the multipole expansions for all boxes in our tree, the next step is to transform the multipole expansion of distant boxes into a local expansion in the observer box. The multiple level approach results in boxes of varying size and we will first consider the case of a childless source box which is larger than the observer box such that the distance between them is larger than the side length of the observer box, but smaller than that of the source box. Assuming there are *n* particles inside the source box, the potential at a point $\mathbf{r}(x,y,z)$ within the observer box at $\mathbf{r}_{\mathrm{o}}'(x_{\mathrm{o}}', y_{\mathrm{o}}', z_{\mathrm{o}}')$, contributed from the particles in the source box, can be expressed as

$$\phi_{\mathrm{L}} = \sum_{i=1}^{n} \frac{q_i}{|\mathbf{r} - \mathbf{r}_i|} = \sum_{i=1}^{n} \frac{q_i}{|\mathbf{r}_{\mathrm{o}}' - \mathbf{r}_i + \mathbf{d}'|},$$

where $\mathbf{d}' = \mathbf{r} - \mathbf{r}_{\mathrm{o}}' = \mathbf{r}'$ and q_i is the charge of the source particle at $\mathbf{r}_i$. Choosing the components of $\mathbf{d}'$ as DA variables, we have the local expansion of the potential. It is called "local", since $\mathbf{r}_{\mathrm{o}}'$ is the center of the observer box and $\mathbf{d}'$ represents the coordinates of the observer with respect to the observer box center.

On the other hand, if the source and observer boxes have the same size and their distance is equal to or greater than their side length, we can convert the multipole expansion in one box into the local expansion in the other one. Assuming that the multipole expansion is expressed as $d \cdot \phi_{\mathrm{M}}$, centered at $\mathbf{O}(0,0,0)$ and the center of the observer box is $\mathbf{r}_{\mathrm{o}}'(x_{\mathrm{o}}', y_{\mathrm{o}}', z_{\mathrm{o}}')$, we can choose the new DA variables as $\mathbf{d}' = \mathbf{r} - \mathbf{r}_{\mathrm{o}}' = \mathbf{r}'$, where $\mathbf{r}'(x', y', z')$ are the new coordinates of the observer $\mathbf{r}(x, y, z)$, by shifting the origin to $\mathbf{r}_{\mathrm{o}}'$. The transformation between the old and the new DA variables, M_2, is given by $\mathbf{d} = \mathbf{r}/r^2 = (\mathbf{r}_{\mathrm{o}}' + \mathbf{r}') \cdot R$ with $R = 1/|\mathbf{r}_{\mathrm{o}}' + \mathbf{d}'|^2$ and $d = \sqrt{R}$. Then the local expansion can be calculated as $\phi_{\mathrm{L}} = (d \cdot \phi_{\mathrm{M}}) \circ M_2 = \sqrt{R} \cdot (\phi_{\mathrm{M}} \circ M_2)$. A child box inherits the local expansion of its parent box because the boxes in the far region of the parent box are also in the far region of the child box. As a result, when calculating the local expansion for a box, one only needs to consider the boxes which are close to the parent of the observer box, increasing the efficiency of the algorithm. To translate the local expansion from the center of the parent box, $\mathbf{O}(0,0,0)$, to the center of the child box, $\mathbf{r}_{\mathrm{o}}'(x_{\mathrm{o}}', y_{\mathrm{o}}', z_{\mathrm{o}}')$, we choose the coordinates of the observer in the child box frame as new DA variables $\mathbf{d}'$. The relation between the old and new DA variables is just a linear shift: $\mathbf{d} = \mathbf{r}_{\mathrm{o}}' + \mathbf{d}'$, which we call the map M_3. The new local expansion is then simply

$$\phi_{\mathrm{L}}' = \phi_{\mathrm{L}} \circ M_3.$$

Now we are ready to calculate the local expansion for all the boxes. Notice that using the local expansion ϕ_L, we actually represent the potential as Taylor expansions of **d**, the coordinates of an observer particle. Taking the derivative of ϕ_L with respect to **d**, which can be performed as a DA intrinsic function, one obtains the field.

There is a remaining special case, which arises when the source box is smaller than the childless observer box and their distance is larger than the side length of the source box but smaller than that of the observer box. In this case we need to calculate the field at the observer particle positions using the multiple expansion $d \cdot \phi_M$ of the source box. To calculate the field we take the derivative with respect to the coordinates and, using the chain rule, we obtain the expression of the field as

$$E_i = \left\{ -\frac{\partial \phi_{\mathrm{M}}}{\partial d_i} \cdot (d^2 - 2d_i^2) + 2\frac{\partial \phi_{\mathrm{M}}}{\partial d_j} \cdot d_i d_j + 2\frac{\partial \phi_{\mathrm{M}}}{\partial d_k} \cdot d_i d_k + \phi_{\mathrm{M}} \cdot d_i \right\} \cdot d \ ,$$

where *i*, *j*, and *k* represent *x*, *y*, or *z*, respectively. As shown above, it is very easy to calculate the expansions using DA variables since one only needs to select the proper small variables that allow representing the potential as a Taylor expansion. The error of the algorithm can be controlled and estimated by looking at the truncation order of the Taylor expansion.

In Figure 2 we compare the computational time required to calculate the 3D space charge field of a bunch of electrons with a Gaussian distribution, using the DA based MLFMA and using the direct calculation of the field by summation of the Coulomb potentials. A linear fit of the data in a logarithmic plot shows that, as expected, the computational time for the direct calculation is proportional to n^2, while the slope of the DA based MLFMA is 1.073, giving a scaling which is very close to being linear in *n* (which would be represented by a slope equal to one). The deviation from linearity is due to the fact that interactions between particles in adjacent boxes are calculated using the pairwise formula for the Coulomb potential. We note that due to the computational overhead associated with the MLFMA, for low numbers of particles ($n < 1000$) the direct calculation usually leads to a lower computational time. However, as the number of particles is increased, the MLFMA vastly outperforms the direct Coulomb summation.

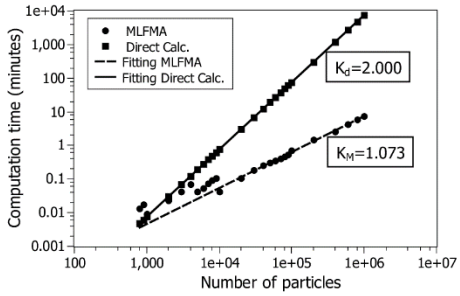

Figure 2. Comparison of the efficiency (computational time) of the DA based MLFMA (DA order 5, relative error < 0.001) with the direct calculation using the pairwise formula for the Coulomb potential.

We now apply the MLFMA implementation to simulations of photoemission of high brightness electron beams. The initial photoemission stage is critical for the operation of ultrafast electron microscopes because the initial phase space volume occupied by the pulse, which is a function of the extraction conditions and the initial Coulomb expansion, determines the achievable temporal and spatial resolutions. As a high number of electrons is required, one must also take into account the so called virtual cathode limit.

We generate the electron bunch through photoemission from a gold photocathode irradiated with a femtosecond laser pulse and describe this process using the so-called three-step photoemission model [19,20] in which each electron is emitted independently as a result of absorbing a photon, diffusing to the surface and escaping to the vacuum. The initial velocities of the electrons are determined by energy considerations and the initial positions are a function of the transverse profile of the laser pulse. The time evolution of the emitted electrons is treated by solving their relativistic equations of motion at each time step using a fourth order Runge-Kutta algorithm and, in addition to the electron-electron interactions, we include an constant extraction field F_a and the positive field generated by the image charge on the cathode surface. For more details see [21-23]. A comparison of our simulations to density profiles of photoemitted electron bunches extracted from shadow imaging experiments [24] shows excellent agreement for the description of the beam dynamics over a wide range of parameters. Our model is able to accurately capture the nonlinear dynamics of the photoemission process and successive propagation of the pulse for varying extraction conditions.

In order to use the generated electron bunch for single-shot diffraction or imaging, the Rose criterion tells us that about 100 electrons per pixel are needed to have a sufficient signal to noise ratio. This means that we need between 10^5 and 10^9 electrons per pulse, so a key quantity of interest is the final number of electrons that escape from the surface. For low laser fluences (total number of photons per unit area), the number of emitted electrons is directly proportional to the fluence, which in the simulation corresponds to the initial number of electrons. As the initial number of electrons is increased, there is a deviation from this linear relationship due to the virtual cathode limit, as the negative charge of the electrons emitted at earlier times hinders further emission. Increasing the extraction field shifts the onset of this phenomenon, allowing extraction of a higher number of particles from the photocathode.

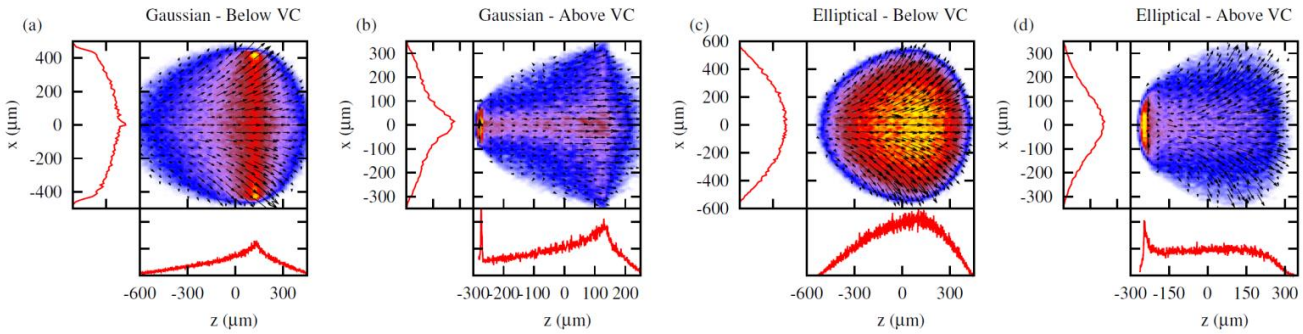

Figure 3. Color map and projection onto the axes of the charge density, overlaid with arrows representing the average electron velocity. All the data corresponds to 10^7 electrons per pulse, extraction fields F_a = 10 MV/m [(a) and (c)] and F_a = 0.32 MV/m [(b) and (d)] respectively.

Figure 3 shows the effects of the virtual cathode (VC) by comparing the charge distribution of the generated electron pulse in its rest frame both above and below the VC limit. Also shown are overlaid arrows representing the average electron velocity and projections onto the *x* and *z* axes. Panels (a) and (b) show data corresponding to a laser pulse with a Gaussian transverse profile [$I(r) \sim exp[-r^2/(2\sigma^2)]$], while panels (c) and (d) were generated using an elliptical laser profile [$I(r) \sim \sqrt{1-(r/\sigma)^2}$]. For conditions below the VC limit [panels (a) and (c)] the flow becomes fully laminar as shown by the uniform distribution of the arrows representing the average electron velocity. The pulse evolves into the typical pancake shape with an ellipsoidal transverse profile. Above the VC limit [panels (b) and (d)], the pulse retains a turbulent flow in the distribution of velocities and does not detach from the surface, as seen in the peak in the density for values of *z* close to the surface, a typical signature of the VC limit.

Varying the photoemission conditions (extraction field, laser profile, laser aspect ratio, etc.) it is possible to compare different regimes of pulse generation and find optimal photoemission conditions that minimize both the transverse and longitudinal emittances [21-23]. Other quantities of interest such as the coherence length and energy spread can also be considered, showing that optimal extraction conditions depend on a delicate balance between the image charge, the number of electrons emitted, the extraction field, which controls the onset of the virtual cathode limit and the aspect ratio of the laser pulse. Through our simulations it is possible to identify ideal operation regimes and extraction fields for pulses with a given charge and provide expected figures of merit for use in the design of the next generation UEMs.

In summary, we have described the steps in the implementation of the MLFMA to handle arbitrary charge distributions in a natural way with a linear scaling of the computational time as a function of the number of particles. We applied the MLFMA to the simulation of photoemission of high brightness electron beams. By varying the extraction conditions, we see evidence of virtual cathode formation and are able to provide guidelines for experimental realizations of UEMs [25].

References:

[1] R Srinivasan *et al*, Helv. Chim. Acta **86** (2003), p. 1763.
[2] A Gahlmann *et al*, Phys. Chem. Chem. Phys. **10** (2008), p. 2894.
[3] B Siwick *et al*, J. Appl. Phys. **92** (2002), p. 1643.
[4] W King *et al*, J. Appl. Phys. **97** (2005), 111101.
[5] T van Oudheusden *et al*, Phys. Rev. Lett. **105** (2010), 264801.
[6] J Rosenzweig *et al*, IEEE T. Plasma. Sci. **24** (1996), p. 409.
[7] S Anderson and J Rosenzweig, Phys. Rev. Spec. Top.-Ac. **3** (2000), 094201.
[8] B Rosenzweig *et al*, Nucl. Instr. Meth. A **557** (2006), p. 87.
[9] Y Li *et al*, Phys. Rev. Spec. Top.-Ac. **12** (2009), 020702.
[10] J Carrier *et al*, SIAM J. Sci. Stat. Comp. **9** (1988), p. 699.
[11] B Shanker and H Huang, J. Comp. Phys. **266** (2007), p. 732.
[12] L Ying *et al*, J. Comp. Phys. **196** (2004), p. 591.
[13] W Fong and E Darve, J. Comp. Phys. **228** (2009), p. 8712.
[14] M Berz in "Modern map methods in particle beam physics", (Academic Press, San Diego, 1999).
[15] M Berz and K Makino, Nucl. Instr. Meth. A **558** (2006), p. 346.
[16] M Berz and K Makino in "COSY INFINITY 9.1 programmer's manual", MSUHEP-101214, (Michigan State University, East Lansing, 2011), http://cosyinfinity.org.
[17] H Zhang and M Berz, Nucl. Instr. Meth. A **645** (2011), p. 338.
[18] H Zhang in "The fast multipole method in the differential algebra framework for the calculation of 3D space charge fields", PhD thesis, (Michigan State University, East Lansing, 2013).
[19] CN Berglund and WE Spicer, Phys. Rev. **136** (1964), p. A1030.
[20] DH Dowell and JF Schmerge, Phys. Rev. Spec. Top.- Ac. **12** (2009), 074201.
[21] J Portman *et al*, Appl. Phys. Lett. **103** (2013), 253115.
[22] J Portman *et al*, J. Appl. Phys. **116** (2014), 174302.
[23] J Portman *et al*, Adv. Imag. Elect. Phys, in press (2015).
[24] Z Tao *et al*, J. Appl. Phys. **111** (2012), 044316.
[25] We acknowledge support from the US National Science Foundation under Grant No. NSF-DMR 1126343 and the US Department of Energy under Grant No. DE-FG02-08ER41546. Computational work was performed at Michigan State University's High Performance Computing Facility.